HHS Public Access

Author manuscript

Neuroimage. Author manuscript; available in PMC 2020 September 01.

Published in final edited form as:

Neuroimage. 2019 September ; 198: 150–159. doi:10.1016/j.neuroimage.2019.05.008.

The effects of psychiatric history and age on self-regulation of the default mode network

Stavros Skouras[1,2] **Frank Scharnowski**[3,4,5]

[1]Neuroimaging Unit, Barcelonabeta Brain Research Center, Pasqual Maragall Foundation, Barcelona, 08005, Spain [2]Department of Experimental and Health Sciences, Pompeu Fabra University, Barcelona, 08005, Spain [3]Department of Psychiatry, Psychotherapy and Psychosomatics, Psychiatric Hospital, University of Zürich, Zürich, 8032, Switzerland [4]Neuroscience Center Zürich, University of Zürich and Swiss Federal Institute of Technology, Zürich, 8057, Switzerland [5]Zürich Center for Integrative Human Physiology (ZIHP), University of Zürich, Winterthurerstr. 190, Zürich, 8057, Switzerland

Abstract

Real-time neurofeedback enables human subjects to learn to regulate their brain activity, effecting behavioral changes and improvements of psychiatric symptomatology. Neurofeedback up-regulation and down-regulation have been assumed to share common neural correlates. Neuropsychiatric pathology and aging incur suboptimal functioning of the default mode network. Despite the exponential increase in real-time neuroimaging studies, the effects of aging, pathology and the direction of regulation on neurofeedback performance remain largely unknown. Using real-time fMRI data shared through the Rockland Sample Real-Time Neurofeedback project (N=136) and open-access analyses, we first modeled neurofeedback performance and learning in a group of subjects with psychiatric history (n_a=74) and a healthy control group (n_b=62). Subsequently, we examined the relationship between up-regulation and down-regulation learning, the relationship between age and neurofeedback performance in each group and differences in neurofeedback performance between the two groups. For interpretative purposes, we also investigated functional connectomics prior to neurofeedback. Results show that in an initial session of default mode network neurofeedback with real-time fMRI, up-regulation and down-regulation learning scores are negatively correlated. This finding is related to resting state differences in the eigenvector centrality of the posterior cingulate cortex. Moreover, age correlates negatively with default mode network neurofeedback performance, only in absence of psychiatric history. Finally, adults with psychiatric history outperform healthy controls in default mode network up-regulation. Interestingly, the performance difference is related to no up-regulation learning in controls. This finding is supported by marginally higher default mode network centrality during resting state, in the presence of psychiatric history.

Corresponding author: Dr. Stavros Skouras. Postal address: Barcelonaβeta Brain Research Center, Carrer de Wellington 30, 08005 Barcelona. Tel: +34 69 30 31 719. Fax +34 93 32 63 192. sskouras@barcelonabeta.org.

Keywords

Learning; Neurofeedback; Real-time; rt-fMRI; ECM

Introduction

Neuroimaging research is contributing considerably to progress towards the apprehension of neurological and psychiatric disorders, by illustrating and characterizing their neural substrates. Current translational efforts are focused on validating non-invasive, neuroimaging-based diagnostic and therapeutic clinical applications. Out of the most innovative technological developments of our time, neurofeedback (NF) based on real-time functional magnetic resonance imaging (rt-fMRI) enables human subjects to learn to self-regulate their brain function, effecting behavioral changes and improvements of clinical symptomatology (Sitaram et al., 2017). Numerous recent studies have demonstrated therapeutic effects of rt-fMRI NF training on chronic pain (deCharms et al., 2005), addiction (Li et al., 2013; Hartwell et al., 2013), Parkinson's disease (Subramanian et al., 2011), stroke (Robineau et al., 2017; Liew et al., 2016), tinnitus (Haller et al., 2010) and depression (Linden et al., 2012; Young et al., 2014; Young et al., 2017); consolidating the view that patients can learn to normalize abnormal patterns of brain activity that are associated with pathology (Sitaram et al., 2017; Stoeckel et al., 2014). Nevertheless, knowledge on the precise mechanisms underpinning the self-regulation of brain function is only nascent at present, and no conclusive theoretical framework for NF learning has been established (Sitaram et al., 2017). Especially in the context of clinical NF applications, the field is still lacking fundamental empirical evidence.

First, it has not been ascertained whether individuals with a history of psychiatric pathology are generally expected to perform equally to healthy participants in self-regulating brain function. Second, the way in which psychiatric pathologies affect specific cognitive requirements of a regulation task is unknown. Third, key performance constraints, such as the effect of age, in relation to self-regulation of brain function and pathology, have not been investigated.

Here we address these three open issues regarding self-regulation of brain function, using the largest publicly available rt-fMRI NF repository, comprising data from healthy participants and psychiatric patients, during bidirectional self-regulation of the default mode network (DMN). The DMN is a large-scale cerebral network (Raichle et al., 2001) associated with a variety of brain functions, including perception (Kelly et al., 2008), attention (Weissman et al., 2006), semantic processing (Binder et al., 2009, Krieger-Redwood et al., 2016; Murphy et al., 2017), divergent thinking (Benedek et al., 2016), self-generation of emotion (Engen et al., 2017) and memory (Mayer et al. 2010; Rugg and Vilberg, 2013; Konishi et al., 2015; Murphy et al., 2018; Spreng et al., 2014; Vatansever et al., 2015), which has become highly relevant for clinical applications (Zhang and Raichle, 2010; Brakowski et al., 2017; Mulders et al., 2015; Hamilton et al., 2015). Similarly to psychiatric pathology, aging also incurs suboptimal functioning of the human brain's DMN (Whitfield-Gabrieli and Ford, 2012; Damoiseaux et al., 2008). Recent studies have

demonstrated that DMN activity can be modulated through NF training (Harmelech et al., 2013; Megumi et al., 2015; Van De Ville et al., 2012). Thus, the DMN provides an optimal neural substratum for investigating the generic self-regulation of brain function.

Based on previous work assuming common neural mechanisms for up-regulation and down-regulation (Emmert et al., 2016) and proposing a generic neurofeedback learning network (Sitaram et al., 2017), we hypothesized that up-regulation and down-regulation learning scores would be positively correlated. Due to previously noted aberrant DMN function in pathological populations (Whitfield-Gabrieli and Ford, 2012), we expected that healthy participants would perform better than psychiatric patients in DMN self-regulation. Because of the impeding effects of aging on DMN function (Damoiseaux et al., 2008), we predicted that age would show a negative correlation with DMN self-regulation performance.

Materials and Methods

Participants

Young adults, aged 20 to 45 years (M = 30.94 years, SD = 7.32, N = 140; 58% female), took part in the study. Participants were residents of the Rockland County (New York, U.S.A.) and participated voluntarily in the Rockland Sample Real-Time Neurofeedback project, a large study aiming to create a sample with extensive neuropsychological and medical profiling, including several functional neuroimaging tasks (McDonald et al., 2017; Nooner et al., 2012). In order to include participants with a range of clinical and sub-clinical symptoms, minimally restrictive exclusion criteria were applied to exclude individuals with severe illnesses that would compromise compliance with experimental instructions (e.g. history of neoplasia requiring intrathecal chemotherapy or focal cranial irradiation, Global Assessment of Function < 50, history of psychiatric hospitalization, or suicide attempts requiring medical intervention). Clinical diagnoses were determined prior to inclusion in the study, by a psychiatrist using SCID-IV criteria (McDonald et al., 2017). Modal psychiatric diagnoses were substance abuse and major depressive disorder, with a high percentage of comorbidity (Figure 1, Table 1). All subjects gave written informed consent; Institutional Review Board Approval was obtained for this project at the Nathan Kline Institute and at Montclair State University (Nooner et al., 2012). Subjects that presented a past or ongoing psychiatric diagnosis comprised the pathological group (M = 30.70 years; SD = 7.17; n_a = 74; 55.4% female; 89.2% dextrous); subjects that had not presented any psychiatric diagnosis comprised the control group (M = 30.71 years; SD = 7.48; n_b = 62; 50% female; 90.3% dextrous); and four unclassified subjects were excluded from further analysis.

Experimental design

Participants completed a variety of assessments and functional neuroimaging tasks comprising the Enhanced Nathan Kline Institute-Rockland Sample (NKI-RS) protocol, described in detail elsewhere (McDonald et al., 2017; Nooner et al., 2012). The protocol included a six-minute resting state fMRI acquisition, followed by a twelve-minute neurofeedback task. Combined with diagnostic and demographic information, these two acquisitions comprised the only datasets of relevance to the present study. Rt-fMRI data

were used to derive neurofeedback performance and neurofeedback learning scores for each participant and for each direction of regulation, via General Linear Modeling (GLM).

Correlation testing was utilized to investigate the relation between DMN up-regulation neurofeedback learning and DMN down-regulation learning scores in the entire sample. Permutation testing was utilized to investigate differences in neurofeedback performance between the experimental group and the control group, for each direction of regulation. Nonparametric correlation testing was used to investigate the relation between neurofeedback performance and age, in each group.

To control for *Type I* error due to performing five individual statistical tests using data from the same sample, we used the Bonferonni correction method (Abdi, 2007) to adjust the typical significance level, $\alpha = 0.05$ (see Statistical analysis). For the typical *Type II* error rate ($\beta = 0.2$), a priori computations of required sample size, using statistical power estimation software (G*Power v 3.1; Heinrich-Heine-Universitat Dusseldorf RRID:SCR_013726; Faul et al., 2007; Faul et al., 2009), confirmed sufficient two-tail statistical power for effects of medium or large size using the entire sample ($d > 0.487$) and for effects of moderate or large size using only the pathological group ($d > 0.660$) or only the control group ($d > 0.727$).

Resting state and neurofeedback task

A resting state acquisition preceded the neurofeedback task because it was required for the delineation of each participant's DMN. During resting state, participants fixated on a white plus (+) sign centered on a black background for six minutes. During the neurofeedback task, stimuli comprised of the neurofeedback display illustrated in Figure 2B, which was implemented using a programming library (Vision Egg RRID:SCR_014589; Straw 2008) and is publicly available online from the 'OpenCogLab Repository' (GitHub; RRID:SCR_002630; https://git.io/vptev). All subjects participated in 12 counterbalanced, alternating trials of DMN up-regulation and down-regulation, of varying length (30 s, 60 s, 90 s). Each type of trial (e.g. up-regulation for 30 s) was repeated twice, once in the first and once in the second block of the session. Participants were instructed at the beginning of each trial to attempt to either let their mind wander (up-regulation), or to focus their attention (down-regulation), while attending to one out of four counterbalanced NF displays (Figure 2A). Counterbalancing was performed with regards to the following: 1) each trial featured a duration of either 30s, 60s or 90s; 2) each trial featured a central instruction, which was either "Focus" or "Wander"; 3) each trial featured the words "Focused" on the left and the word "Wandering" on the right or vice versa.

MRI data acquisition

Scanning was performed with a 3 T Siemens Magnetom TIM Trio scanner (Siemens Medical Solutions, Malvern, PA, USA) using a 12-channel head coil. Before the functional MR measurements, a fast localizer and high-resolution anatomical sequence were acquired. Anatomical images were acquired using a 3D T1-weighted MPRAGE (Mugler and Brookeman, 1990) GRAPPA (Griswold et al., 2002) sequence with an acceleration factor of 2 and 32 reference lines. 192 sagittal partitions were acquired, each of a 256×256 field of

view (FOV), using a 2600 ms repetition time (TR), a 3.02 ms echo time (TE), 900 ms inversion time (TI) and 8° flip angle (FA), resulting in a 1 mm^3 isomorphic voxel resolution.

Functional scanning included a six-minute resting state, comprised of 182 volumes and a 12-minute neurofeedback task, comprised of 412 volumes. The resting state scan was performed before the neurofeedback task and both scanning sequences featured the same scanning parameters. The overall acquisition protocol featured additional functional tasks (e.g. moral dilemma task; McDonald et al., 2017), which were of no relevance to the present study. Functional images were acquired using echo planar imaging (EPI) with a TE of 30 ms, FA 90° and a TR of 2010 ms. Slice-acquisition was interleaved within the TR interval. The matrix acquired was 64×64 voxels with a FOV of 220 mm, resulting in an in-plane resolution of 3.4×3.4 mm^2. Slice thickness was 3.6 mm with an interslice gap of 0.36 mm (30 slices). Images were exported over a network interface (Cox et al., 1995; LaConte et al., 2007). Physiological measures including galvanic skin response, pulse oximetry, rate of breathing and depth of breathing were measured during functional acquisitions.

MRI data processing

Prior to the NF session, the DMN of each participant had been delineated, based on the data from the resting state scan, using standard fMRI data preprocessing (McDonald et al., 2017) and Support Vector Regression (SVR) with the 3dsvm tool (LaConte et al., 2005), which is based on the SVMlight implementation of machine learning (Joachims, 1999). The procedure used a whole-brain template of the DMN derived from independent component analysis of the 29,671-subject BrainMap activation database (Smith et al., 2009; Fox & Lancaster, 2002; Laird et al., 2005) to extract a weighted timeseries of DMN activity from the resting state data of each participant. The DMN timeseries and the resting state data of each participant were submitted to 3dsvm (similarly to Craddock et al., 2013) resulting in a customized DMN mask for each participant (McDonald et al., 2017). Prior to the NF task, the whole-brain DMN template (Smith et al., 2009) had been used to compute normalization transforms between the native space of each participant's anatomical acquisition and the MNI stereotactic space. This facilitated denoising during the neurofeedback task, when white matter and cerebrospinal fluid signals were regressed out of the rt-fMRI data and the SVR model, that was pre-trained on the resting state data, was used to estimate the DMN activation of each participant, for each real-time TR, using 3dsvm combined with other software routines from AFNI (Analysis of Functional Neuroimages v 18.1.05; National Institute of Mental Health RRID:SCR_005927; Cox, 1996; LaConte et al., 2005) and FSL (FMRIB Software Library v 5.0; Oxford Centre for Functional MRI of the Brain RRID:SCR_002823; Zhang et al., 2001; Jenkinson et al., 2002; Jenkinson and Smith, 2001; Greve and Fischl, 2009; Greve and Fischl, 2009). A two-stage approach was used for motion correction whereby images were coregistered to the mean fMRI volume and then a new mean volume was calculated and used as the target for a second coregistration using AFNI 3dvolreg (Turner et al., 2003; McDonald et al., 2017). Following discretization, the real-time estimates of DMN activation produced by 3dsvm were converted to angular positions of a needle on a tachometer-like NF display, according to four experimental designs that were counterbalanced across participants (Figure 2B).

All neuroimaging data had been subjected to the ‘Preprocessed Connectomes Project Quality Assessment Protocol’ (GitHub; RRID:SCR_002630; https://git.io/vptfA; Shehzad et al., 2015) to compute spatial and temporal quality measures, in order to validate or discard acquisitions. Data had been curated on and were accessed via the Collaborative Informatics and Neuroimaging Suite Data Exchange (COINS; Mind Research Network RRID:SCR_000805; Scott et al., 2011; Wood et al., 2014). The data featured a neurofeedback logfile for each participant, summarizing the measures of moment-to-moment neurofeedback performance derived by the real-time processing pipeline that was applied during data acquisition. The neurofeedback logfile for each participant was programmatically retrieved and read into computer memory using software (Matlab v 9.3; Mathworks RRID:SCR_001622). Structured variables were constructed to store all relevant information, regarding each participant's and each trial's characteristics. Hypothesis testing was performed as described in section ‘Statistical analysis’ and as illustrated in complete detail in the publicly available computer program developed for the analysis (see Code accessibility).

To investigate DMN connectivity patterns at baseline, the DMN template that was also used in the real-time NF pipeline (Smith et al. 2009) was thresholded above 3.719, corresponding to $P < 0.0001$, to maintain a z-map that featured only the main regions of the DMN (i.e. posterior cingulate cortex/precuneus, medial prefrontal cortex, inferior parietal lobules, lateral temporal cortices; Figure 5A). Resting state data were processed in raw data units using the MIT Connectivity Toolbox (CONN; RRID:SCR_009550). The data processing pipeline featured registration of T1-weighted anatomical data to the functional dataset for each participant, realignment and reslicing of functional data, identification of movement artifacts using the Artifact Detection Tools (ART; RRID:SCR_005994) and movement thresholds equal to voxel width. Anatomical data were segmented using the ‘New Segmentation’ algorithm (SPM12; RRID:SCR_007037). Functional data were denoised via regression of mean white matter signal, mean cerebrospinal fluid signal, 24 Volterra expansion movement parameters and scannulling regressors (Lemieux et al., 2007) produced by ART. Additional processing was implemented via a combination of specialized open-source software tools. SyGN (Avants, Tustison, et al., 2010; Tustison and Avants, 2013) from the Advanced normalization Tools (ANTs; version 2.x, committed in January 2016; http://stnava.github.io/ANTs/; RRID:SCR_004757; Avants et al., 2009) was used to compute neuroanatomically plausible symmetric diffeomorphic matrices and transform each subject's anatomical data to the ICBM MNI brain template that features sharp resolution, detailed gyrification and high signal-to-noise ratio, while minimizing abnormal anatomy biases (Fonov et al., 2011). The cranium of the ICBM template had been removed in advance, similarly as for the anatomical data, prior to the normalization of datasets. Normalized resolution was limited to $3\times3\times3$ mm^3 due to restrictions posed by computational demands. Functional data were filtered using a temporal highpass filter with a cutoff frequency of 1/90 Hz, smoothed with a 3D Gaussian kernel of 6 mm FWHM and subjected to the computationally intensive Eigenvector Centrality Mapping (ECM; Lohmann et al., 2010; Wink et al., 2012) using the Leipzig Image Processing and Statistical Inference Algorithms (LIPSIA; version 2.2.7 – released in May 2011; Max Planck Institute for Human Cognitive and Brain Sciences, Leipzig, Germany; http://www.cbs.mpg.de/institute/software/lipsia;

RRID:SCR_009595; Lohmann et al., 2000), similarly to previous studies (Koelsch & Skouras, 2014; Taruffi et al. 2017; Skouras et al. 2019). ECM was preferred over other methods because it as an assumption-free, data-driven approach with solid grounding on advanced graph theory that effectively reflects patterns of whole-brain functional connectomics (Borgatti, 2005; Bonacich & Lloyd, 2004; Lohmann et al., 2010; Wink et al., 2012). To enable parametric testing, ECM z-maps were gaussianized (Albada & Robinson, 2007) and subjected to statistical tests as described in the section 'Statistical analysis'.

Code accessibility

All original code developed for the analysis has been made available to any researcher for purposes of reproducing or extending the analysis, via the 'NKI_RS_analysis' public repository (GitHub; RRID:SCR_002630; https://git.io/vxddI). Following download, the main analysis and progressive output can be viewed on any browser (HTML version) or replicated and modified interactively using the Live Editor in Matlab v 9.3 or higher (MLX version).

Data accessibility

Neuroimaging data, further described in (McDonald et al., 2017), are available online via the Neuroimaging Informatics Tools Resources Clearinghouse (NITRC; RRID:SCR_003430). Diagnostic assessment data are available following the completion of a data transfer agreement with the Nathan Kline Institute (Nathan S. Kline Institute for Psychiatric Research; New York; USA, RRID:SCR_004334) via the Collaborative Informatics and Neuroimaging Suite Data Exchange (COINS; Mind Research Network RRID: SCR_000805).

Statistical analysis

Standard general linear modeling was employed to quantify NF performance and learning. Using Pearson's r as a metric of similarity, actual NF moment-to-moment regulation, as captured by the angular position of a needle on a tachometer-like NF display (Figure 2B), was compared to a linear vector representing the target performance of the experimental design (Figure 2C), producing a measure of NF performance for each of the 12 experimental trials. For each participant, average NF scores were computed separately for DMN up-regulation trials (wander), and DMN down-regulation trials (focus), in each of the two experimental blocks. NF learning score was computed as the improvement in NF regulation from the first to the second block of the session. NF performance score was computed as the average correlation between target performance and actual NF regulation in the second block of the session (following the introductory block of the session which comprised the participants' very first practice experience of NF and of each trial type). Lilliefors test (Lilliefors, 1969) was used to assess normality and Grubbs' test (Grubbs, 1969) was used for outlier detection. Parametric correlation testing was used to assess the relation between DMN up-regulation learning and DMN down-regulation learning score, because the variables were normally distributed. Non-parametric correlation testing was used to assess the relation between overall neurofeedback performance and age, because the distribution of age deviated from normality. Permutation testing was used to assess differences in neurofeedback performance scores between the experimental and control groups. Detailed

documentation of the analysis, along with explanatory comments and an interactive program have been made available to facilitate replication and in support of the Open Science Initiative. Five statistical tests were performed in total. To control for *Type I* error due to performing multiple statistical tests using data from the same sample, we used the Bonferonni correction method (Abdi, 2007) and set the adjusted two-tail significance level to $\alpha = 0.005$.

For interpretative purposes and due to previous evidence (Scheinost et al., 2014) we investigated whether our main findings could be supported by pre-NF resting state DMN connectivity. The general systematic approach was to attempt to replicate effects on neurofeedback performance with respective effects involving average pre-NF DMN Eigenvector Centrality (EC). With regards to EC, small-volume analyses, were followed by voxel-wise second-level GLM, to exclude the possibility of subregion-specific effects within the DMN. All voxel-wise tests were corrected for multiple comparisons at $P < 0.05$ using 10,000 Monte Carlo permutations with a cluster forming threshold set to $z > 2.3$, similarly to previous studies (Lohmann et al., 2010; Nierhaus 2015). Regarding the relation between DMN up-regulation learning and DMN down-regulation learning scores, we performed correlation tests between average pre-NF DMN metrics and self-regulation learning scores, separately for up-regulation and down-regulation. Neurofeedback learning scores had been orthogonalized in relation to age and the experimental group factor, to utilize the entire sample while controlling for the influence of these variables, using the recursive Gram-Schmidt orthogonalisation of basis functions implemented in SPM12.

Results

Direction of regulation

Lilliefors testing (Lilliefors, 1969) showed that NF up-regulation learning and down-regulation learning scores did not deviate from normality. Further quality assurance using Grubbs' test for outlier detection (Grubbs, 1969) showed that no outliers were present in any utilized variables. Parametric correlation testing revealed that DMN NF up-regulation learning ($M = 0.135$, $SD = 0.554$, $N = 136$) and down-regulation learning scores ($M = 0.189$, $SD = 0.587$) were significantly negatively correlated, with a weak association explaining approximately 7% of the variance, $r(136) = -0.258$, $R^2 = 0.067$, $P = 0.0024$; Figure 3A.

Controlling for the effects of age and pathology, average pre-NF DMN EC did not correlate with NF up-regulation, nor down-regulation, $P > 0.05$. Voxel-wise GLM, corrected for multiple comparisons using 10,000 Monte Carlo permutations, showed that pre-NF resting state EC in the Posterior Cingulate Cortex (PCC) and Precuneus (PCu) correlated positively with up-regulation learning [$r(136) = 0.989$, $R^2 = 0.978$, $P < 0.00001$ uncorrected; Figure 5B; Table 2] and negatively with down-regulation learning [$r(136) = -0.986$, $R^2 = 0.972$, $P < 0.00001$ uncorrected; Figure 5B ; Table 3]. Apart from the PCC/PCu, two additional clusters, in the anterior cingulate cortex and cerebellum correlated positively with up-regulation learning, and two other clusters, in the subgenual anterior cingulate cortex and medial prefrontal cortex, correlated negatively with down-regulation learning; Tables 2-3. Supplementary 3D neuroimaging data include MNI-registered NIfTI images of these results for visualization and usage as regions of interest in future studies.

Age

Lilliefors testing showed that the distribution of age (M = 30.71 years, SD = 7.28, N = 136) deviated from normality. Non-parametric correlation testing using Spearman's correlation coefficient revealed that in the pathological group, age (M = 30.70 years; SD = 7.17; n_a = 74) had no effect on overall neurofeedback performance (M = 0.333, SD = 0.301), $r(74)$ = −0.0711, P = 0.547. In the control group, age (M = 30.71 years; SD = 7.48; n_b = 62) correlated negatively with overall DMN NF performance score (M = 0.195, SD = 0.312) with a moderate association that explained 17% of the variance, $r(62)$ = −0.412, R^2 = 0.17, P = 0.0009; Figure 3B.

Age did not correlate significantly with average pre-NF DMN EC, in neither the pathological nor the control group, (P > 0.05). Voxel-wise GLM, corrected for multiple comparisons using 10,000 Monte Carlo permutations, revealed that age had distinct effects in the two groups on resting state functional connectomics, however these effects were not localized within the DMN (Supplementary Figures S1-S2; Supplementary Tables 1-2). Supplementary 3D neuroimaging data include MNI-registered NIfTI images of these results for visualization and usage as regions of interest in future studies.

Psychiatric pathology

Non-parametric independent samples t-tests, with 100,000 permutations per test, revealed that participants with a psychiatric history performed significantly better in DMN NF up-regulation (M = 0.383, SD = 0.420, n_a = 74) than the control group (M = 0.159, SD = 0.467, n_b = 62), $t(134)$ = −2.951, P = 0.0036; d = 0.504; Figure 4A. Down-regulation performance was not significantly different between participants with a psychiatric history (M = 0.283, SD = 0.385) and the control group (M = 0.232, SD = 0.462), $t(134)$ = −0.711, P = 0.479. The difference in up-regulation performance was due to a lack of learning, with regards to up-regulation (mind-wandering), in the control group; Figure 4B.

An ROI analysis of DMN EC, using gaussianized ECM z-maps revealed marginally higher DMN EC in the pathological group, t(134)=1.884, p=0.031, d=0.324. Voxel-wise GLM, corrected for multiple comparisons using 10,000 Monte Carlo permutations, revealed ECM differences between the two groups, however these effects were not localized within the DMN (Supplementary Figure S3; Supplementary Table 3). Supplementary 3D neuroimaging data include MNI-registered NIfTI images of these results for visualization and usage as regions of interest in future studies. Neurofeedback scores across diagnostic categories are displayed in Figure 6.

Discussion

In relation to existing questions of fundamental importance to self-regulating brain function, we have shown that initial learning of DMN self-regulation is influenced by age and psychiatric history, as well as by pre-NF differences in EC. Specifically, during an initial, brief DMN rt-fMRI NF session, participants with a psychiatric history outperform healthy controls in DMN up-regulation. Further, age correlates negatively with the ability to self-regulate DMN function. Finally, up-regulation learning and down-regulation learning scores

are negatively correlated in both patients and healthy controls and partly determined by pre-NF EC of the PCC/PCu.

A negative effect of age on DMN self-regulation is not surprising, given that reduced connectivity within the DMN's PCC and medial prefrontal cortex has been observed in normal aging (Andrews-Hanna et al. 2007; Sambataro 2010), due to decreasing DMN integrity (Dennis & Thompson, 2014). The DMN also comprises the primary locus of earliest amyloid deposition due to aging in cognitively normal individuals (Dennis & Thompson, 2014; Palmqvist et al., 2017). Although it does not affect cognitive performance, such a neurobiological burden poses limitations on the neural efficiency of the DMN, leading to functional connectivity changes (Palmqvist et al., 2017) and age-related decline in task-related modulation of DMN activity (Sambataro et al., 2010). Our finding indicates that in healthy subjects, age explains 17% of the variation in NF self-regulation scores. This strong effect is even more remarkable considering that the age range in our study was limited to young adults (20-45 years of age), similarly to most NF studies to date. Hence, age must be considered and explicitly modeled when assessing the ability to self-regulate brain function.

Although no previous rt-fMRI study investigated age effects on rt-fMRI NF performance, our finding corroborates complementary evidence, regarding self-regulation, from electrophysiological biofeedback and neurofeedback studies. Heart rate variability biofeedback performance has been reported to correlate negatively with age and the effects of biofeedback self-regulation training on cardiovascular measures were less pronounced in older subjects (Lehrer et al., 2006). EEG theta amplitude up-regulation was also illustrated to be noticeably better in young compared to old subjects, although that study did not investigate performance differences between age groups via statistical testing (Wang and Hsieh, 2013).

DMN activity has been linked primarily to occipital alpha band activity (Jann et al., 2010) that is known to decrease with age (Breslau et al., 1989), substantiating a plausible physiological basis for the effects observed here. It should be noted that despite the evidence for decreased self-regulation performance in older subjects, the beneficial effects of neurofeedback and biofeedback self-regulation training on cognitive and respiratory function, are stronger in elders (Lehrer et al., 2006; Wang and Hsieh, 2013), suggesting the suitability of self-regulation training as a promising intervention to support healthy aging.

A surprising finding from our study relates to the absence of an age effect in the pathological group. In cohort with the complementary finding of better performance in the pathological group, our results suggest that good self-regulation performance is not necessarily reflecting healthy brain function. Our results imply that higher up-regulation performance in the pathological group was likely due to higher ECM in the DMN at baseline, especially because higher ECM in the DMN at baseline was also associated with better up-regulation learning. This corroborates previous evidence of pathologically altered DMN function (Broyd et al., 2009) and may be associated to reduced DMN coherence due to increased DMN connectivity with the rest of the brain. Indeed our ECM results suggest that the DMN is more interconnected with the rest of the brain in the pathological group and in this sense

less coherent as an independent resting state network. These new findings suggest that generic hypotheses of reduced performance and reduced connectivity in pathological populations need to be revisited.

It is worth considering that the capacity to show improvement in NF performance is contingent upon aberrant baseline activity. That is, when NF is used to normalize brain activity in patients that present moderately abnormal, aberrant activity, the patients will probably perform better than controls that present normal, stable activity patterns. On the other hand, in the face of severe pathology that impairs fundamental learning capacities, the ability to improve NF performance will be impaired as well, although this was not the case for the high-functioning pathological group of the present study.

The third important finding of our study is that initial learning of DMN self-regulation is unidirectional, with the amount of learning in one direction of regulation opposing learning in the other direction of regulation and explaining 7% of its variation. In this study, up-regulation was associated with mind-wandering strategies and down-regulation with focusing attention. Thus, our findings suggest that learning to self-regulate depends on task-specific performance constraints rather than a more generic ability to self-regulate. This may partly explain why the search for general predictors of successful neurofeedback learning has not been successful so far and why the proportion of up to 30% of participants that fail to self-regulate effectively, even following extensive practice (Harmelech et al., 2015), varies between targeted brain regions and paradigms (Sitaram et al., 2017). In order to design improved experimental and clinical protocols, it is critical to consider the direction of regulation, task-specific peculiarities, and individual predispositions such as pre-NF functional connectomics in target regions.

It remains possible that the present findings may be influenced by unaccounted factors that are not homogeneously distributed across the two experimental groups or across the age range of the sample. These may include experience with types of training that can exert a covert influence on the ability to self-regulate physiological processes; e.g. meditational practice, musical training, acting experience etc. (Gruzelier, 2014a, 2014b). It is possible that, on average, the pathological group had received more training in self-regulation of cognitive and physiological functions through participation in cognitive behavioral therapy programs. Moreover, it remains possible that our findings are limited only to the DMN and only to initial sessions of self-regulation. Future research should systematically investigate learning effects in cardinal brain networks (i.e. default mode, executive control and salience networks) across several sessions using identical protocols.

A potential experimental limitation is that even though focusing was meant to drive down-regulation of the DMN, focusing on thoughts of personal relevance, such as auto-biographical events or autobiographical planning can lead to increased DMN activity (Gusnard et al., 2001; Addis et al., 2007; Spreng et al., 2010; Spreng et al., 2015) and that we did not possess quantifiable information on the extent of focusing on such thoughts across participants. Therefore, it cannot be ascertained that the observed effects are not partly attributable to structured variation in the level of focusing on self-oriented thoughts. Arguably, clinical populations and especially patients with major depressive disorder, spend

an increased amount of time performing mind-wandering and self-referential rumination, compared to non-clinical populations. This may result in enhancing the ability to up-regulate the DMN and suggests that appropriately designed DMN NF paradigms may serve in producing clinically relevant neuromarkers. On the other hand, in contrast to task-fMRI paradigms that elicit DMN activation, in the context of neurofeedback tasks and with the aid of real-time neurofeedback displays, participants learn to avoid using mental strategies with negative impact on the neurofeedback performance. Moreover, the ability of both groups to improve on down-regulation (focusing) supports that they did not differ in terms of the level of self-referential cognition during focus trials (Figure 4B). Nevertheless, the level of self-referential thinking should be quantified and modeled in future DMN NF studies. Moreover, future studies on the self-regulation of the DMN, should consider using different or complementary instructions that relate down-regulation to attending to one's immediate environment and up-regulation to internally mediated cognition. Such studies could aid in clarifying the specificity and interindividual variability of DMN functions.

In conclusion, we have illustrated that participants with a psychiatric history can perform better than healthy controls in self-regulating brain function. The ability to up-regulate brain function appears to decrease with age only in the absence of psychiatric history, and good performance in learning to up-regulate the DMN through one cognitive task does not imply equally good performance in down-regulating the DMN through another cognitive task. The latter is evidenced by the negative correlation between up-regulation learning and down-regulation learning, which are partly explained by PCC/PCu functional connectomics during resting state. Although it remains to be determined to what extent these findings are specific to the DMN and to initial sessions of self-regulation through rt-fMRI NF, our findings contribute to the furtherment of neurophysiological knowledge and our understanding of the neural mechanisms underpinning self-regulation of brain function specifically. We anticipate that our findings will solidify the foundations for more systematic modeling of the self-regulation of brain function and assist in the design of advanced technologies and experimental protocols for clinical applications.

Supplementary Material

Refer to Web version on PubMed Central for supplementary material.

Acknowledgements

This work was supported by the European Union's Horizon 2020 research and innovation programme under the Marie Sklodowska-Curie action grant agreement No 707730, the Foundation for Research in Science and the Humanities at the University of Zurich (STWF-17-012), the Baugarten Stiftung, and the Swiss National Science Foundation (BSSG10_155915, 32003B_166566). Principal support for the Rockland Sample Real-Time Neurofeedback project was provided by the NIMH BRAINS R01-MH101555 (PI Craddock). The authors thank Cameron Craddock for insightful discussions. The authors declare no competing financial interests.

References

Abdi H 2007 Bonferroni and Šidák corrections for multiple comparisons. Encyclopedia of measurement and statistics 3: 103–107.

Addis DR, Wong AT, Schacter DL. 2007 Remembering the past and imagining the future: Common and distinct neural substrates during event construction and elaboration. Neuropsychologia 45(7): 1363–1377. [PubMed: 17126370]

Albada VS, Robinson PA. 2007 Transformation of arbitrary distributions to the normal distribution with application to EEG test–retest reliability. Journal of neuroscience methods 161: 205–211. [PubMed: 17204332]

Andrews-Hanna JR, Reidler JS, Sepulcre J, Poulin R, Buckner RL. 2010 Functional-anatomic fractionation of the brain's default network. Neuron 65(4):550–562. [PubMed: 20188659]

Avants BB, Epstein CL, Grossman M, Gee JC. 2008 Symmetric diffeomorphic image registration with crosscorrelation: evaluating automated labeling of elderly and neurodegenerative brain. Medical image analysis 12: 26–41. [PubMed: 17659998]

Avants BB, Tustison N, Song G. 2009 Advanced normalization tools (ANTS). Insight 2: 1–35.

Avants B, Tustison N, Song G, Cook P, Klein A, Gee J. 2010 A reproducible evaluation of ANTs similarity metric performance in brain image registration. NeuroImage 54: 2033–44. [PubMed: 20851191]

Avants B, Yushkevich P, Pluta J, Minkoff D, Korczykowski M, Detre J, et al. 2010 The optimal template effect in hippocampus studies of diseased populations. NeuroImage 49: 2457–2466. [PubMed: 19818860]

Benedek M, Jauk E, Beaty RE, Fink A, Koschutnig K, Neubauer AC. 2016 Brain mechanisms associated with internally directed attention and self-generated thought. Sci. Rep. 6: 22959 [PubMed: 26960259]

Binder JR, Desai RH, Graves WW, Conant LL. 2009 Where is the semantic system? A critical review and metaanalysis of 120 functional neuroimaging studies. Cerebral Cortex 19(12): 2767–2796. [PubMed: 19329570]

Borgatti SP. 2005 Centrality and network flow. Social networks 27: 55–71.

Bonacich P, Lloyd P. 2004 Calculating status with negative relations. Social Networks 26 (4): 331–338.

Brakowski J, Spinelli S, Dorig N, Bosch OG, Manoliu A, Holtforth MG, Seifritz E. 2017 Resting state brain network function in major depression - Depression symptomatology, antidepressant treatment effects, future research. J Psychiatr Res 92, 147–159. [PubMed: 28458140]

Breslau J, Starr A, Sicotte N, Higa J, Buchsbaum MS. 1989 Topographic EEG changes with normal aging and SDAT. Electroencephalogr. Clin Neurophysiol 72: 281–289. [PubMed: 2467793]

Broyd SJ, Demanuele C, Debener S, Helps SK, James CJ, Sonuga-Barke EJS. 2009 Default-mode brain dysfunction in mental disorders: a systematic review. Neurosci Biobehav Rev 33: 279–296. [PubMed: 18824195]

Cox RW, Jesmanowicz A, Hyde JS. 1995 Real-time functional magnetic resonance imaging. Magn Reson Med 33: 230–236. [PubMed: 7707914]

Cox RW. 1996 Afni software for analysis and visualization of functional magnetic resonance neuroimages. Comput Biomed Res 29: 162–173. [PubMed: 8812068]

Craddock CR, Milham MP, LaConte SM. 2013 Predicting intrinsic brain activity. NeuroImage 82: 127–136. [PubMed: 23707580]

Damoiseaux JS, Beckmann CF, Arigita EJS, Barkhof F, Scheltens P, Stam CJ, Smith SM, Rombouta SARB. 2008 Reduced resting-state brain activity in the ‘default network’ in normal aging. Cereb Cortex 18: 1856–1864. [PubMed: 18063564]

deCharms RC, Maeda F, Glover GH, Ludlow D, Pauly JM, Soneji D, Gabrieli JDE, Mackey SC. 2005 Control over brain activation and pain learned by using real-time functional MRI. Proc Natl Acad Sci U S A 102: 18626–18631. [PubMed: 16352728]

Dennis EL, Thompson PM. 2014 Functional brain connectivity using fMRI in aging and Alzheimer’s disease. Neuropsychol Rev 24: 49–62. [PubMed: 24562737]

Emmert K, Kopel R, Sulzer J, Brühl AB, Berman BD, Linden DEJ, Horovitz SG, Breimhorst M, Caria A, Frank S, Johnston S, Long Z, Paret C, Robineau F, Veit R, Bartsch A, Beckmann CF, Van De Ville D, Haller S. 2016 Metaanalysis of real-time fMRI neurofeedback studies using individual participant data: How is brain regulation mediated? NeuroImage 124: 806–812. [PubMed: 26419389]

Engen HG, Kanske P, Singer T. 2017 The neural component-process architecture of endogenously generated emotion. Soc. Cognit. Affect Neurosci, 12 (2): 197–211. [PubMed: 27522089]

Faul F, Erdfelder E, Lang AG, Buchner A. 2007 G*Power 3: A flexible statistical power analysis program for the social, behavioral, and biomedical sciences. Behavior Research Methods 39: 175–191. [PubMed: 17695343]

Faul F, Erdfelder E, Buchner A, Lang AG. 2009 Statistical power analyses using G*Power 3.1: Tests for correlation and regression analyses. Behavior Research Methods, 41, 1149–1160. [PubMed: 19897823]

Fonov V, Evans AC, Botteron K, Almli RC, McKinstry RC, Collins LD. 2011 Unbiased average age-appropriate atlases for pediatric studies. NeuroImage 54: 313–327. [PubMed: 20656036]

Fox PT, Lancaster JL. 2002 Mapping context and content: The BrainMap model. Nat Rev Neurosci 3:319–321. [PubMed: 11967563]

Greve DN, Fischl B. 2009 Accurate and robust brain image alignment using boundary-based registration. NeuroImage 48: 63–72. [PubMed: 19573611]

Griswold MA, Jakob PM, Heidemann RM, Nittka M, Jellus V, Wang J, Kiefer B, Haase A. 2002 Generalized autocalibrating partially parallel acquisitions (grappa). Magn Reson Med 47: 1202–1210. [PubMed: 12111967]

Grubbs F 1969 Procedures for Detecting Outlying Observations in Samples. Technometrics 11: 1–21.

Gurven M et al. 2017 Cognitive performance across the life course of Bolivian forager-farmers with limited schooling. Dev Psychol 53: 160–176. [PubMed: 27584668]

Gusnard DA, Akbudak E, Shulman GL, Raichle ME. 2001 Medial prefrontal cortex and self-referential mental activity: Relation to a default mode of brain function. Proceedings of the National Academy of Sciences of the United States of America 98(7): 4259–4264. [PubMed: 11259662]

Gruzelier JH. 2014 EEG-neurofeedback for optimising performance. I: a review of cognitive and affective outcome in healthy participants. Neurosci Biobehav Rev 44: 124–141. [PubMed: 24125857]

Gruzelier JH. 2014 EEG-neurofeedback for optimising performance. II: creativity, the performing arts and ecological validity. Neurosci Biobehav Rev 44: 142–158. [PubMed: 24239853]

Haller S, Birbaumer N, Veit R. 2010 Real-time fMRI feedback training may improve chronic tinnitus. Eur Radiol 20: 696–703. [PubMed: 19760238]

Hamilton JP, Farmer M, Fogelman P, Gotlib IH. 2015 Depressive rumination, the default-mode network, and the dark matter of clinical neuroscience. Biol Psychiatry 78: 224–230. [PubMed: 25861700]

Harmelech T, Friedman D, Malachvolume R. 2015 Differential magnetic resonance neurofeedback modulations across extrinsic (visual) and intrinsic (default-mode) nodes of the human cortex. J Neurosci 35: 2588–2595. [PubMed: 25673851]

Harmelech T, Preminger S, Wertman E, Malach R. 2013 The day-after effect: long term, Hebbian-like restructuring of resting-state fMRI patterns induced by a single epoch of cortical activation. J Neurosci 33: 9488–9497. [PubMed: 23719815]

Hartwell KJ, Prisciandaro JJ, Borckardt J, Li XB, George MS, Brady KT. 2013 Real-Time fMRI in the treatment of nicotine dependence: a conceptual review and pilot studies. Psychol Addict Behav 27: 501–509. [PubMed: 22564200]

Heberle H, Meirelles GV, da Silva FR, Telles GP, Minghim R. 2015 InteractiVenn: a web-based tool for the analysis of sets through Venn diagrams. BMC Bioinformatics 16:169. [PubMed: 25994840]

Jann K, Kottlow M, Dierks T, Boesch C, Koenig T. 2010 Topographic electrophysiological signatures of fMRI resting state networks. PLoS One 5: e12945. [PubMed: 20877577]

Jenkinson M, Smith S. 2001 A global optimisation method for robust affine registration of brain images. Med Image Anal 5: 143–156. [PubMed: 11516708]

Jenkinson M, Bannister P, Brady M, Smith S. 2002 Improved optimization for the robust and accurate linear registration and motion correction of brain images. NeuroImage 17: 825–841. [PubMed: 12377157]

Kelly AM, Uddin LQ, Biswal BB, Castellanos FX, Milham MP. 2008 Competition between functional brain networks mediates behavioral variability. NeuroImage 39: 527–537. [PubMed: 17919929]

Koelsch S, Skouras S. 2014 Functional centrality of amygdala, striatum and hypothalamus in a "small-world" network underlying joy: An fMRI study with music. Human brain mapping 35(7): 3485–3498. [PubMed: 25050430]

Konishi M, McLaren DG, Engen H, Smallwood J. 2015 Shaped by the past: the default mode network supports cognition that is independent of immediate perceptual input. PLoS One 10(6): e0132209. [PubMed: 26125559]

Krieger-Redwood et al. 2016 Down but not out in posterior cingulate cortex: Deactivation yet functional coupling with prefrontal cortex during demanding semantic cognition. NeuroImage 141: 366–377. [PubMed: 27485753]

LaConte SM, Strother SC, Cherkassky V, Anderson J, Hu X. 2005 Support vector machines for temporal classification of block design fmri data. NeuroImage 26: 317–329. [PubMed: 15907293]

LaConte SM, Peltier SJ, Hu XP. 2007 Real-time fmri using brain-state classification. Hum Brain Mapp 28: 1033–1044. [PubMed: 17133383]

Laird A, Lancaster J, Fox P. 2005 BrainMap. The social evolution of a human brain mapping database. NeuroInformatics 3:65–77. [PubMed: 15897617]

Lehrer P, Vaschillo E, Lu SE, Eckberg D, Vaschillo B, Scardella A, Habib R. 2006 Heart rate variability biofeedback: effects of age on heart rate variability, baroreflex gain, and asthma. Chest 129: 278–284. [PubMed: 16478842]

Lemieux L, Salek-Haddadi A, Lund TE, Laufs H. 2007 Modelling large motion events in fMRI studies of patients with epilepsy. Magnetic resonance imaging 25:894–901. [PubMed: 17490845]

Li X, Hartwell KJ, Borckardt J, Prisciandaro JJ, Saladin ME, Morgan PS, Johnson KA, LeMatty T, Brady KT, George MS. 2013 Volitional reduction of anterior cingulate cortex activity produces decreased cue craving in smoking cessation: a preliminary real-time fMRI study. Addict Biol 18: 739–748. [PubMed: 22458676]

Liew SL, Rana M, Comelsen S, de Barros MF, Birbaumer N, Sitaram R, Cohen LG, Soekadar SR. 2016 Improving Motor Corticothalamic Communication After Stroke Using Real-Time fMRI Connectivity-Based Neurofeedback. Neurorehabilit Neural Repair 30: 671–675.

Lilliefors H 1969 On the Kolmogorov-Smirnov test for the exponential distribution with mean unknown. J Am Stat Assoc 64: 387–389.

Linden DEJ, Habes I, Johnston SJ, Linden S, Tatineni R, Subramanian L, Sorger B, Healy D, Goebel R. 2012 Realtime self-regulation of emotion networks in patients with depression. PLoS One 7: e38115. [PubMed: 22675513]

Lohmann G, Müller K, Bosch V, Mentzel H, Hessler S (2000): LIPSIA-Leipzig Image Processing and Statistical Inference Algorithms.

Lohmann G, Margulies DS, Horstmann A, Pleger B, Lepsien J, Goldhahn D, et al. 2010 Eigenvector centrality mapping for analyzing connectivity patterns in fMRI data of the human brain. PloS one 5: e10232. [PubMed: 20436911]

Mayer JS, Roebroeck A, Maurer K, Linden DEJ. 2010 Specialization in the Default Mode: Task-Induced Brain Deactivations Dissociate Between Visual Working Memory and Attention. Hum Brain Mapp 31: 126–139. [PubMed: 19639552]

McDonald AR et al. 2017 The real-time fMRI neurofeedback based stratification of Default Network Regulation Neuroimaging data repository. NeuroImage 146: 157–70. [PubMed: 27836708]

Megumi F, Yamashita A, Kawato M, Imamizu H. 2015 Functional MRI neurofeedback training on connectivity between two regions induces long-lasting changes in intrinsic functional network. Front Hum Neurosci 9: 160. [PubMed: 25870552]

Mulders PC, van Eijndhoven PF, Schene AH, Beckmann CF, Tendolkar I. 2015 Resting-state functional connectivity in major depressive disorder: A review. Neurosci Biobehav Rev 56: 330–344. [PubMed: 26234819]

Murphy C, et al. 2017 Fractionating the anterior temporal lobe: MVPA reveals differential responses to input and conceptual modality. NeuroImage 147: 19–31. [PubMed: 27908787]

Murphy C, et al. 2018 Distant from input: Evidence of regions within the default mode network supporting perceptually-decoupled and conceptually-guided cognition. NeuroImage 171:393–401. [PubMed: 29339310]

Nierhaus T, et al. 2015 Imperceptible somatosensory stimulation alters sensorimotor background rhythm and connectivity. Journal of Neuroscience 35(15):5917–5925. [PubMed: 25878264]

Nooner KB et al. 2012 The NKI-Rockland sample: a model for accelerating the pace of discovery science in psychiatry, Front Neurosci 6: 152. [PubMed: 23087608]

Palmqvist S, Scholl M, Strandberg O, Mattsson N, Stomrud E, Zetterberg H, Blennow K, Landau S, Jagust W, Hansson O. 2017 Earliest accumulation of β-amyloid occurs within the default-mode network and concurrently affects brain connectivity. Nature Comm 8: 1214.

Raichle ME, MacLeod AM, Snyder AZ, Powers WJ, Gusnard DA, Shulman GL. 2001 A default mode of brain function. Proc Natl Acad Sci U S A 98: 676–682. [PubMed: 11209064]

Robineau F, Saj A, Neveu R, Van De Ville D, Scharnowski F, Vuilleumier P. 2017 Using real-time fMRI neurofeedback to restore right occipital cortex activity in patients with left visuo-spatial neglect: proof-of-principle and preliminary results. Neuropsychol Rehabilitation: 1–22.

Rugg MD, Vilberg KL. 2013 Brain networks underlying episodic memory retrieval. Current Opinion in Neurobiology 23(2): 255–260. [PubMed: 23206590]

Salthouse TA. 2003 Interrelations of Aging, Knowledge, and Cognitive Performance In: Staudinger U, Lindenberger U, editors. Understanding Human Development: Dialogues with Lifespan Psychology. New York: Springer p 265–287

Sambataro F, Murty VP, Callicott JH, Tan H, Das S, Weinberger DR, Mattay VS. 2010 Age-related alterations in default mode network: impact on working memory performance. Neurobiol Aging 31: 839–852. [PubMed: 18674847]

Scheinost D, Stoica T, Wasylink S, Gruner P, Saksa J, Pittenger C, & Hampson M. 2014 Resting state functional connectivity predicts neurofeedback response. Frontiers in Behavioral Neuroscience 338.

Scott A, Courtney W, Wood D, de la Garza R, Lane S, King M, Wang R, Roberts J, Turner JA, Calhoun VD. 2011 Coins: An innovative informatics and Neuroimaging Tool Suite Built for Large Heterogeneous Datasets, Front Neuroinformation 5.

Shehzad Z, Giavasis S, Li Q, Benhajali Y, Yan C, Yang Z, Milham M, Bellec P, Craddock RC. 2015 The preprocessed connectomes project quality assessment protocol - a resource for measuring the quality of mri data. Front Neuroscience 9.

Sitaram R, Ros T, Stoeckel L, Haller S, Scharnowski F, Lewis-Peacock J, Weiskopf N, Blefari ML, Rana M, Oblak E, Birbaumer N, Sulzer J. 2017 Closed-loop brain training: the science of neurofeedback. Nature Rev Neurosci 18: 86–100. [PubMed: 28003656]

Skouras S, Falcon C, Tucholka A, Rami L, Sanchez-Valle R, Llado A, Gispert JD, Molinuevo JL. 2019 Mechanisms of functional compensation, delineated by eigenvector centrality mapping, across the pathophysiological continuum of Alzheimer's disease. NeuroImage: Clinical 22: 101777. [PubMed: 30913531]

Smith SM, Fox PT, Miller KL, Glahn DC, Fox PM, Mackay CE, Filippini N, Watkins KE, Toro R, Laird AR, Beckmann CF. 2009 Correspondence of the brain's functional architecture during activation and rest, Proc Natl Acad Sci U S A 106: 13040–13045. [PubMed: 19620724]

Spreng RN, Grady CL. 2010 Patterns of brain activity supporting autobiographical memory, prospection, and theory of mind, and their relationship to the default mode network. Journal of Cognitive Neuroscience 22(6):1112–1123. [PubMed: 19580387]

Spreng RN, DuPre E, Selarka D, Garcia J, Gojkovic S, Mildner J, Turner GR et al. 2014 Goal-congruent default network activity facilitates cognitive control. J. Neurosci, 34 (42): 14108–14114. [PubMed: 25319706]

Spreng RN, Gerlach KD, Turner GR, Schacter DL. 2015 Autobiographical planning and the brain: activation and its modulation by qualitative features. J. Cognit. Neurosci. 27(11): 2147–2157. [PubMed: 26102226]

Stoeckel LE et al. 2014 Optimizing real time fMRI neurofeedback for therapeutic discovery and development. Neuromage Clin 5: 245–255.

Straw AD. 2008 Vision egg: an open-source library for realtime visual stimulus generation. Front NeuroInformatics 2: 4.

Subramanian L, Hindle JV, Johnston S, Roberts MV, Husain M, Goebel R, Linden D. 2011 Real-time functional magnetic resonance imaging neurofeedback for treatment of Parkinson's Disease. J Neurosci 31: 16309–16317. [PubMed: 22072682]

Taruffi L, Pehrs C, Skouras S, Koelsch S. 2017 Effects of sad and happy music on mind-wandering and the default mode network. Scientific reports 7(1): 14396. [PubMed: 29089542]

Turner DC, Robbins TW, Clark L, Aron AR, Dowson J, Sahakian BJ. 2003 Cognitive enhancing effects of modafinil in healthy volunteers. Psychopharmacology 165(3): 260–269. [PubMed: 12417966]

Tustison NJ, Avants BB. 2013 Explicit B-spline regularization in diffeomorphic image registration. Frontiers in neuroinformatics 7: 39. [PubMed: 24409140]

Van De Ville D, Jhooti P, Haas T, Kopel R, Lovblad K, Scheffler K, Haller S. 2012 Recovery of the default mode network after demanding neurofeedback training occurs in spatio-temporally segregated subnetworks. NeuroImage 63: 1775–1781. [PubMed: 22960086]

Vatansever D, Menon DK, Manktelow AE, Sahakian BJ, Stamatakis EA. 2015 Default mode network connectivity during task execution. NeuroImage 122: 96–104. [PubMed: 26220743]

Wang JR, Hsieh S. 2013 Neurofeedback training improves attention and working memory performance. Clin Neurophysiology 124: 2406–2420.

Weissman DH, Roberts KC, Visscher KM, Woldorff MG. 2006 The neural bases of momentary lapses in attention. Nature Neurosci 9: 971–978. [PubMed: 16767087]

Wink AM, de Munck JC, van der Werf YD, van den Heuvel OA, Barkhof F. 2012 Fast eigenvector centrality mapping of voxel-wise connectivity in functional magnetic resonance imaging: implementation, validation, and interpretation. Brain connectivity 2(5): 265–274. [PubMed: 23016836]

Whitfield-Gabrieli S, Ford JM. 2012 Default mode network activity and connectivity in psychopathology. Annu Rev Clin Psychol 8: 49–76. [PubMed: 22224834]

Wood D, King M, Landis D, Courtney W, Wang R, Kelly R, Turner JA, Calhoun VD. 2014 Harnessing Modern Web Application Technology to Create Intuitive and Efficient Data Visualization and Sharing Tools, Front Neuroinformation 8.

Young KD, Siegle GJ, Zotev V, Phillips R, Misaki M, Yuan H, Drevets WC, Bodurka J. 2017 Randomized Clinical Trial of Real-Time fMRI Amygdala Neurofeedback for Major Depressive Disorder: Effects on Symptoms and Autobiographical Memory Recall. Am J Psychiatry 174: 748–755. [PubMed: 28407727]

Young KD, Zotev V, Phillips R, Misaki M, Yuan H, Drevets WC, Bodurka J. 2014 Real-time FMRI neurofeedback training of amygdala activity in patients with major depressive disorder. PLoS One 9: e88785. [PubMed: 24523939]

Zhang Y, Brady M, Smith S. 2001 Segmentation of brain mr images through a hidden markov random field model and the expectation-maximization algorithm. IEEE Trans Med Imaging 20: 45–57. [PubMed: 11293691]

Zhang D, Raichle ME. 2010 Disease and the brain's dark energy. Nature Rev Neurol 6: 15–28. [PubMed: 20057496]

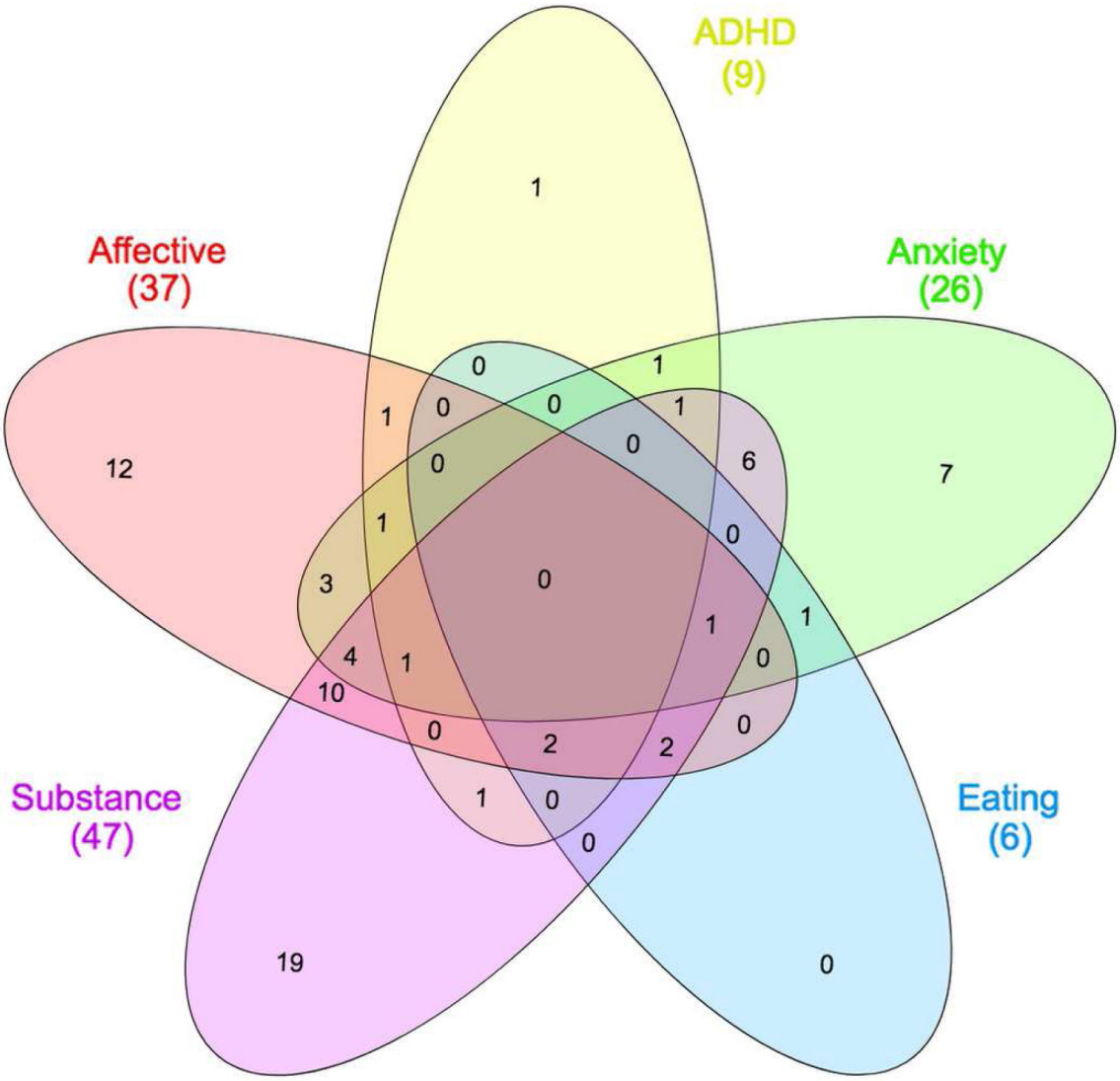

Figure 1. Comorbidity of clinical diagnoses.

Venn diagram illustrating the total number of cases for each category of disorders and detailing cases of comorbid pathology involving disorders from different categories. Visualization performed using InteractiVenn (Heberle et al., 2015). Color coding is in concordance with Figure 6: pink ~ affective disorders; yellow ~ ADHD; green ~ anxiety disorders; blue ~ eating disorders; purple ~ substance use disorder.

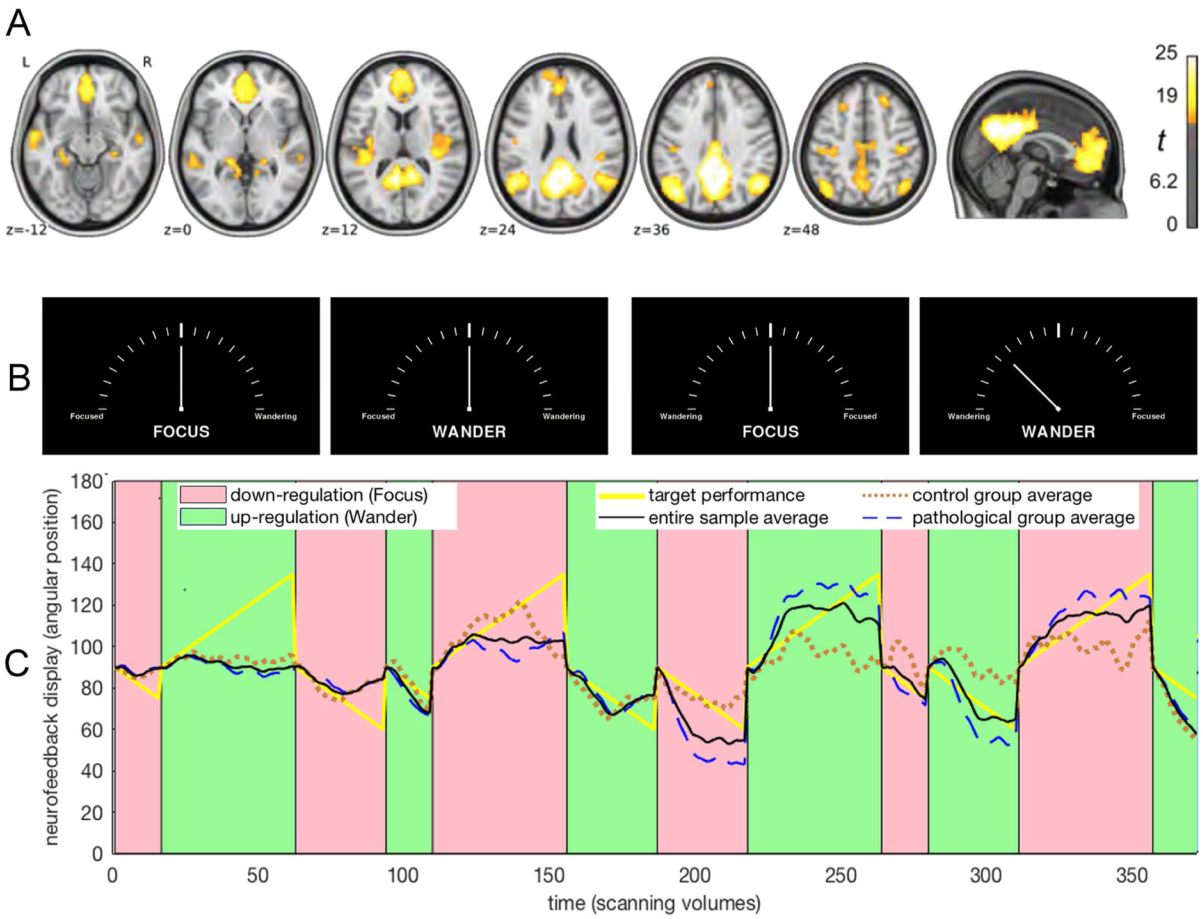

Figure 2. Modeling regulation performance.

A, Spatial map of the average default mode network in the utilized repository (reprinted with permission, from McDonald et al. 2017). **B**, Each experimental trial featured one of the four counterbalanced displays resembling tachometers. At the beginning of each trial, the angular position of the needle pointer was set to 90° and was updated with every new functional volume according to real-time regulation performance; e.g. the rightmost display shows an angular position of 135°. **C**, The graph shows the average default mode network neurofeedback regulation performance for the pathological group (dashed blue line; N=74), for the control group (dotted brown line; N=62) and for the entire sample (black line; N=136), against target performance (yellow line), in one of four counterbalanced trial orders. It is apparent that on average, learning occurred for both up-regulation and down-regulation and that performance improved noticeably in the second half of the real-time fMRI scanning session.

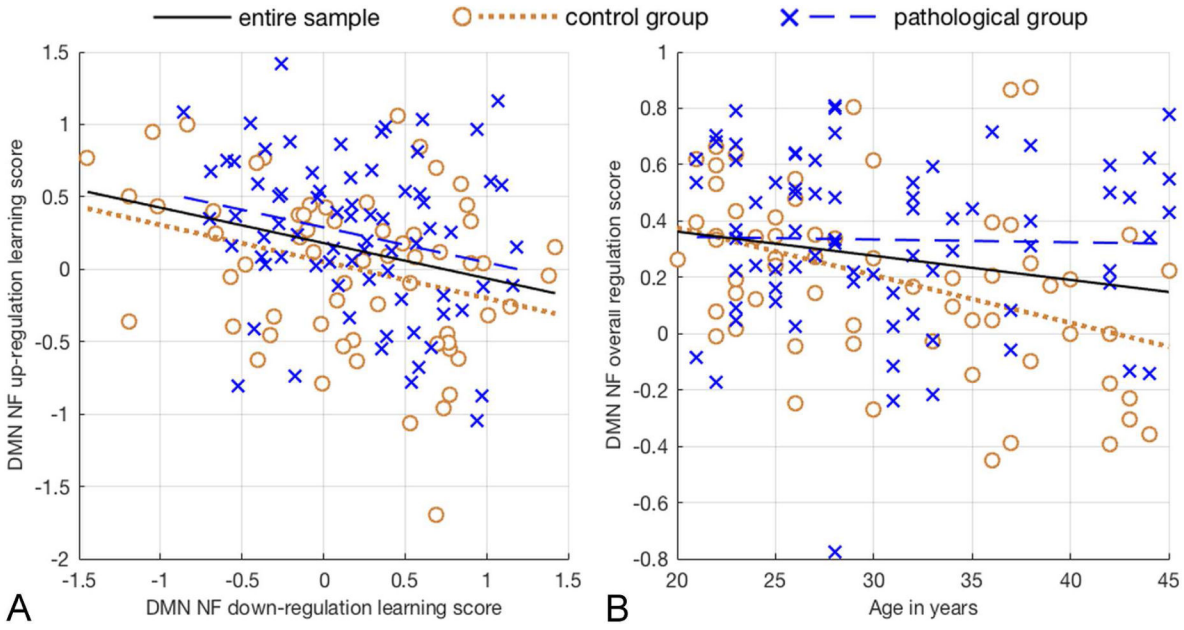

Figure 3. Illustration of the correlation tests performed.

A, The figure shows lines of best fit for the pathological group (dashed blue line; N=74), the control group (dotted brown line; N=62) and the entire sample (black line; N=136). Default mode network neurofeedback up-regulation and down-regulation learning, are negatively correlated [r=−0.258, R^2=0.067, p=0.0024]. **B**, Default mode network neurofeedback regulation performance decreases with age only in psychiatrically healthy adults [r=−0.412, R^2=0.17, p=0.0009].

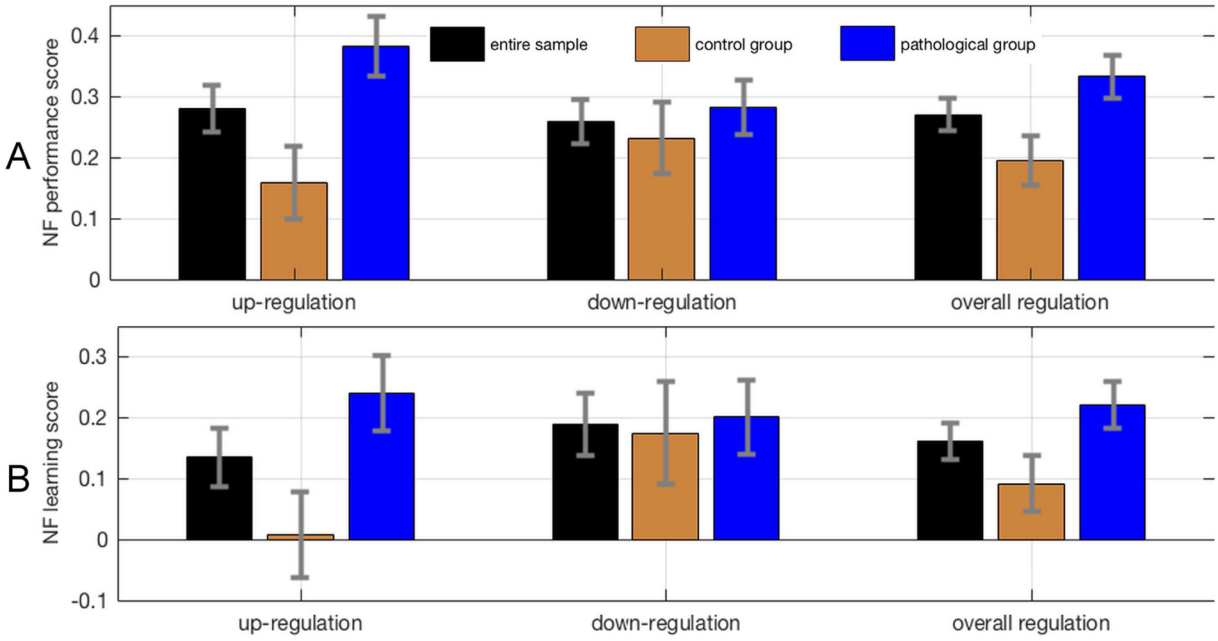

Figure 4. Neurofeedback scores across experimental groups.

A, Neurofeedback performance and neurofeedback learning scores for up-regulation, down-regulation and overall regulation. Scores are depicted separately for the control group, the pathological group and the entire sample. Error bars represent standard errors. Possible neurofeedback performance scores range from a value of −1 (corresponding to worst possible performance) to a value of 1 (corresponding to best possible performance). **B**, Possible neurofeedback learning scores range from a value of −2 (corresponding to worsening performance) to a value of 2 (corresponding to maximal learning).

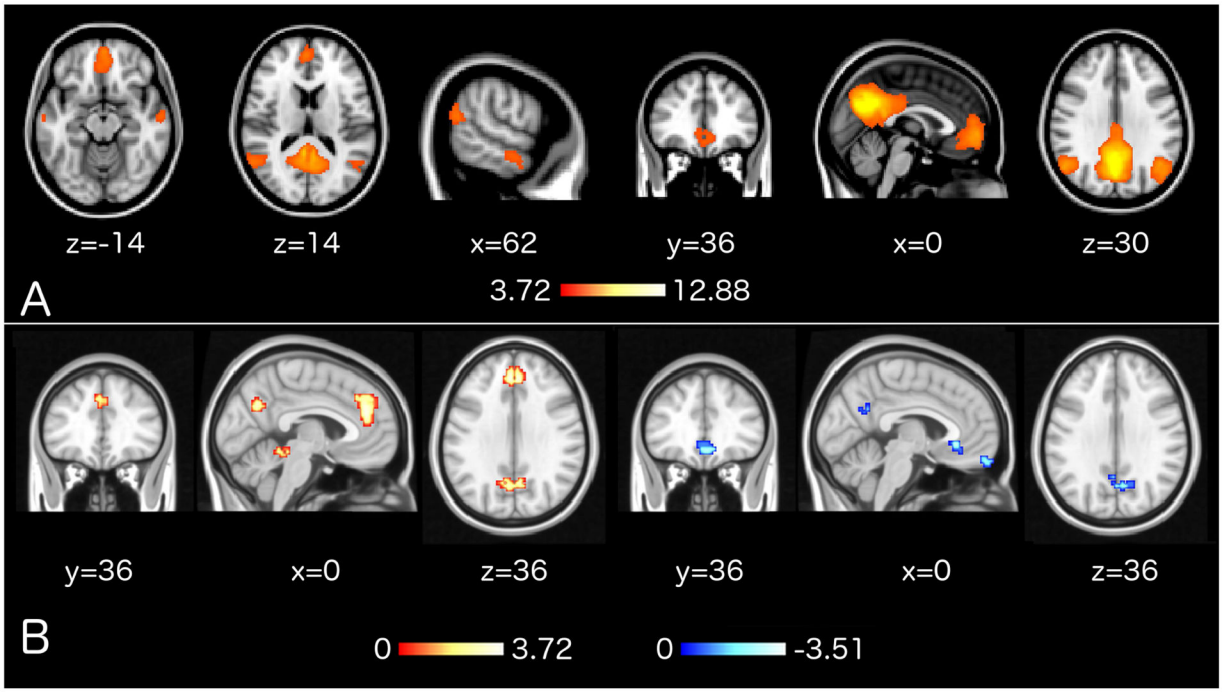

Figure 5. Pre-NF resting state results.

A, Thresholded version (z > 3.72) of the DMN template (Smith et al., 2009) that was used for SVR training prior to neurofeedback. For interpretative purposes, the same template was used for network of interest analyses on pre-NF resting state acquisitions. **B**, Correlations between ECM during pre-NF resting state acquisitions and subsequent neurofeedback learning scores, corrected for whole-brain multiple comparisons using 10,000 Monte Carlo permutations (z > 2.3; P < 0.05). EC in red-yellow clusters correlated positively with up-regulation learning and EC in blue-white clusters correlated negatively with down-regulation learning. Colormap values are in z-scores and coordinates in MNI space.

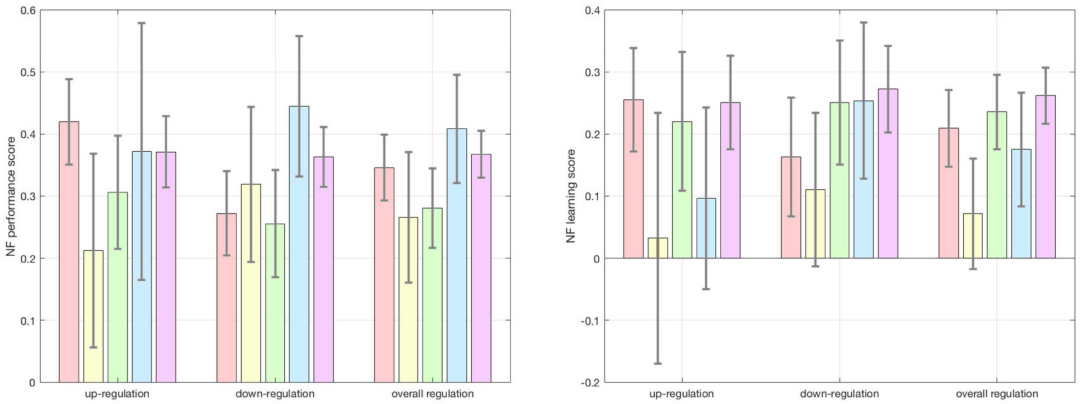

Figure 6. Neurofeedback scores across diagnostic categories.

A, Neurofeedback performance and neurofeedback learning scores for up-regulation, down-regulation and overall regulation. Scores are depicted sequentially, from left to right, for affective disorders, ADHD, anxiety disorders, eating disorders and substance abuse. Error bars represent standard errors. Possible neurofeedback performance scores range from a value of −1 (corresponding to worst possible performance) to a value of 1 (corresponding to best possible performance). **B**, Possible neurofeedback learning scores range from a value of −2 (corresponding to worsening performance) to a value of 2 (corresponding to maximal learning). Color coding is in concordance with Figure 1: pink ~ affective disorders; yellow ~ ADHD; green ~ anxiety disorders; blue ~ eating disorders; purple ~ substance use disorder.

Table 1.
Prevalence of clinical diagnoses in the pathological group.

Specific diagnoses were grouped into five main categories for visualization purposes. Many participants were diagnosed with more than one specific diagnosis from the same disorder category or other disorder categories.

Disorder category	Specific diagnosis	Count
Affective		**38**
	Major Depressive Disorder Single Episode In Full Remission	14
	Major Depressive Disorder Recurrent In Full Remission	12
	Major Depressive Disorder Single Episode Unspecified	4
	Major Depressive Disorder Recurrent Moderate	3
	Dysthymic Disorder	2
	Bereavement	2
	Major Depressive Disorder Recurrent Severe Without Psychotic Features	1
ADHD		**10**
	Attention-Deficit/Hyperactivity Disorder Predominantly Inattentive Type	4
	Attention-Deficit/Hyperactivity Disorder Combined Type	2
	Attention-Deficit/Hyperactivity Disorder NOS	3
	Attention-Deficit/Hyperactivity Disorder Predominantly Hyperactive-Impulsive Type	1
Anxiety		**31**
	Posttraumatic Stress Disorder	7
	Specific Phobia	6
	Generalized Anxiety Disorder	4
	Anxiety Disorder NOS	3
	Panic Disorder With Agoraphobia	3
	Obsessive-Compulsive Disorder	2
	Social Phobia	2
	Panic Disorder Without Agoraphobia	2
	Agoraphobia Without History of Panic Disorder	2
Eating		**6**
	Body Dysmorphic Disorder	2
	Anorexia Nervosa	2
	Bulimia Nervosa	1
	Eating Disorder NOS	1
Substance		**72**
	Alcohol Abuse	26
	Alcohol Dependence	9
	Cannabis Abuse	12
	Cannabis Dependence	12
	Cocaine Abuse	3
	Cocaine Dependence	3

Disorder category	Specific diagnosis	Count
	Amphetamine Abuse	1
	Amphetamine Dependence	1
	Hallucinogen Abuse	1
	Hallucinogen Dependence	1
	Sedative Hypnotic or Anxiolytic Dependence	1
	Opioid Abuse	1
	Polysubstance Dependence	1

Table 2.

Correlations between ECM during resting state and subsequent neurofeedback up-regulation learning.

Up-regulation learning scores, had been orthogonalised with regards to age and psychiatric pathology, to control for confounding effects. Results are corrected for whole-brain multiple comparisons using 10,000 Monte Carlo permutations ($z > 2.3$, $P < 0.05$). The outermost right column indicates the maximal z-value of voxels within a cluster (with the mean z-value of all voxels within a cluster in parentheses). Abbreviations: ACC: Anterior Cingulate Cortex; PCC: Posterior Cingulate Cortex; PCu: Precuneus.

	MNI coord.	cluster size (mm^3)	z-value: max (mean)
ACC	−3 39 28	4320	3.73 (2.74)
PCC/PCu	6 −63 34	1620	3.21 (2.62)
Cerebellum	−6 −42 −11	729	3.05 (2.62)

Table 3.

Correlations between ECM during resting state and subsequent neurofeedback down-regulation learning.

Down-regulation learning scores, had been orthogonalised with regards to age and psychiatric pathology, to control for confounding effects. Results are corrected for whole-brain multiple comparisons using 10,000 Monte Carlo permutations ($z > 2.3$, $P < 0.05$). The outermost right column indicates the maximal z-value of voxels within a cluster (with the mean z-value of all voxels within a cluster in parentheses). Abbreviations: PCC: Posterior Cingulate Cortex; PCu: Precuneus; mPFC: medial Prefrontal Cortex; sACC: subgenual Anterior Cingulate Cortex.

	MNI coord.	cluster size (mm^3)	z-value: max (mean)
PCC/PCu	3 −63 25	1053	−2.82 (−2.46)
sACC	−3 27 −2	1026	−3.15 (−2.61)
mPFC	−12 54 −17	1107	−3.51 (−2.78)